





Article

A Nonlinear Active Disturbance Rejection Feedback Control Method for Proton Exchange Membrane Fuel Cell Air Supply Subsystems

Jiaming Zhou ¹, Weixiang Ding ¹, Jinming Zhang ^{1,*}, Fengyan Yi ², Zhiming Zhang ³, Guangping Wu ⁴ and Caizhi Zhang ⁵

¹ School of Intelligent Manufacturing, Weifang University of Science and Technology, Weifang 262700, China; zhoujiaming@wfust.edu.cn (J.Z.); mdwx3147621@163.com (W.D.)

² School of Automotive Engineering, Shandong Jiaotong University, Jinan 250357, China; yi_fengyan@163.com

³ School of Automotive Studies, Tongji University, Shanghai 201804, China; zhangzm@tongji.edu.cn

⁴ Zhongtong Bus Co., Ltd., Liaocheng 252000, China; pingguangwu1989@163.com

⁵ College of Mechanical and Vehicle Engineering, Chongqing University, Chongqing 400044, China; czzhang@cqu.edu.cn

* Correspondence: zhangjinming@wfust.edu.cn

Abstract: The control strategy of the gas supply subsystem is very important to ensure the performance and stability of the fuel cell system. However, due to the inherent nonlinear characteristics of the fuel cell gas supply subsystem, the traditional control strategy is mainly based on proportional integral (PI) control, which has the disadvantages of large limitation, large error, limited immunity, and inconsistent control performance, which seriously affects its effectiveness. In order to overcome these challenges, this paper proposes an optimal control method for air supply subsystems based on nonlinear active disturbance rejection control (ADRC). Firstly, a seven-order fuel cell system model is established, and then, the nonlinear ADRC and traditional PI control strategies are compared and analyzed. Finally, the two strategies are simulated and compared. The validation results indicate that the integral absolute error (IAE) measure of PI control is 0.502, the integral square error (ISE) measure is 0.1382, and the total variation (TV) measure is 399.1248. Compared with the PI control, the IAE and ISE indexes of ADRC were reduced by 61.31% and 58.03%, respectively. ADRC is superior to PI control strategy in all aspects and realizes the efficient adjustment of the system under different working conditions. ADRC is more suitable for the nonlinear characteristics of the gas supply system and is more suitable for the oxygen excess ratio (OER).

Keywords: proton exchange membrane fuel cell; air supply subsystem; oxygen excess ratio; active disturbance rejection control



check for updates

Citation: Zhou, J.; Ding, W.; Zhang, J.; Yi, F.; Zhang, Z.; Wu, G.; Zhang, C. A Nonlinear Active Disturbance Rejection Feedback Control Method for Proton Exchange Membrane Fuel Cell Air Supply Subsystems. *Actuators* **2024**, *13*, 268. <https://doi.org/10.3390/act13070268>

Academic Editor: Ioan Ursu

Received: 18 June 2024

Revised: 9 July 2024

Accepted: 12 July 2024

Published: 14 July 2024



Copyright: © 2024 by the authors. Licensee MDPI, Basel, Switzerland. This article is an open access article distributed under the terms and conditions of the Creative Commons Attribution (CC BY) license (<https://creativecommons.org/licenses/by/4.0/>).

1. Introduction

Since the advent of the industrial revolution and the widespread use of fossil fuels, the global imperative has been to mitigate environmental pollution and minimize the consumption of finite, non-renewable resources. In pursuit of carbon neutrality, the automotive industry has recognized new energy vehicles as a significant pathway for advancement. With their capability for efficient and clean energy conversion, fuel cells have emerged as a prominent technology in this domain. Fuel cell vehicles (FCVs) represent a crucial aspect of the advancement of new energy vehicles, boasting features such as zero pollution, exceptional energy conversion efficiency, and impressive driving range [1]. The development of FCVs has been the subject of extensive research and development efforts, with significant progress being made in harnessing their potential benefits. These vehicles not only provide an environmentally friendly alternative to traditional fuel sources but also offer improved performance capabilities that cater to the needs of modern consumers. In essence, FCVs

have emerged as a viable solution to the pressing challenges faced by the automotive industry, positioning themselves as a key player in the transition towards sustainable transportation. PEMFCs have promising programs within fields inclusive of transportation, aerospace, and stationary energy systems [2]. With the developing international call for environmentally pleasant and sustainable transportation solutions, fuel cells are gaining interest as an easy and green manner of transportation [3].

FCVs offer notable advantages such as high energy efficiency, extended driving ranges, and zero emissions, making them a highly sought-after research direction within the electric vehicle domain [4–6]. Among various types of fuel cells, PEMFCs are gaining significant attention because of their benefits such as operation at low temperatures, rapid start-up capability, and high power density [7]. As the primary power source, PEMFCs are required to deliver power to vehicles swiftly and consistently [8]. However, system disturbances can lead to delays in the air supply subsystem, resulting in oxygen depletion [9], which accelerates the degradation in PEMFC lifespan. PEMFCs consist of subsystems such as gas supply systems, hydrothermal management systems, and power conditioning systems [10]. The air supply system, among these subsystems, plays a paramount role by providing the necessary oxygen for the electrochemical reactions and facilitating the timely removal of reaction product water. This sustains the continuous progress of the electrochemical reaction.

An effective air supply control system is crucial in delivering a precise OER and pressure ratio to the fuel cell. It ensures optimal oxygen supply while preventing issues such as oxygen deficiency or excessive supply. The control system exhibits the ability to swiftly adjust the air supply in response to rapid changes in fuel cell load. It maintains high precision and reliability during prolonged operation, reducing faults and minimizing downtime. However, traditional linear control methods face limitations when dealing with the nonlinear characteristics and complex operational environment of fuel cell air supply subsystems. Consequently, there is an urgent need to develop a control strategy that can effectively adapt to the system's nonlinear characteristics. This strategy ensures appropriate oxygen supply, robustness, and efficient and stable operation across various operational levels. In the research on control strategies for air supply subsystems, earlier studies mainly used linear controllers as the dominant controllers. Rodatz et al. [11] designed a linear square Gaussian regulator to control the cathode pressure of a PEMFC and verified the effectiveness of the proposed control strategy through experiments and simulations, demonstrating how adjusting airflow can optimize fuel cell performance. She et al. [12] developed a multi-objective controller based on a recursive neural network model to track set values and enhance durability simultaneously. Bianchi et al. [13] proposed a linear parameter-varying gain-scheduling control strategy to adjust the stoichiometry of PEMFCs. Gruber et al. [14] combined the gas delivery subsystem model with a predictive control model. Research shows that predictive model checking can provide good results for accurate models. Nevertheless, obtaining precise models for systems is generally challenging. Laghrouche et al. [15,16], considering the air supply subsystem, employed the sliding mode control method, which is effective in systems with uncertain parameters.

Most studies have proposed various control strategies through the abovementioned models, using the OER or air pressure as control variables. Ma et al. [17] and others introduced an airflow control method based on uncertainty and disturbance estimation, achieving OER tracking control. Abbaker et al. [18] used time-delay control in adjusting the optimal air mixture to enhance the reaction rate and performance of PEMFCs, verified through simulations. Additionally, Hu et al. [19] suggested a robust nonlinear three-step controller design method, validated through simulations. Liu et al. [20,21] and others analyzed OER control and fault reconstruction based on sliding mode techniques, overlooking the dynamics of the backpressure valve, thus being unable to simultaneously control pressure and airflow in the studies mentioned. These studies offer valuable references for the application of nonlinear feedback control in PEMFCs. The control of the cathode-side OER has consistently been a topic of extensive discussion. Wu et al. [22] proposed a method

utilizing a hyperbolic tangent function within an extended state observer to accurately estimate the cathode gas pressure in a fuel cell gas supply system. Deng et al. [23] combines the strengths of LSTM and MPC in developing MPC using an LSTM neural network for modelling and controlling the PEMFC gas supply system. Li et al. [24] proposed a coordinated controller that effectively regulates the OER and air pressure. Their approach is based on input–output linearization and sliding mode methods. The OER value plays a crucial role in impacting the dynamic response capabilities of the PEMFC. It is essential to maintain an appropriate OER to avoid insufficient air supply. An OER value greater than 1 is necessary for ensuring adequate oxygen supply. However, excessive airflow can lead to increased parasitic power consumption within the system. Therefore, it is crucial to control the OER within a reasonable range to strike a balance between ensuring sufficient oxygen supply and minimizing parasitic power consumption. Model predictive control shows difficulty in handling complex systems, has long prediction range problems [25], and requires a large number of calculations to perform predictive control during operation. PI control [26] struggles to ensure robustness under operating conditions [27]. Sliding mode control sometimes exhibits chatter during operation, and model dependence and condition dependence can often limit the effectiveness of these control strategies [28]. The cumbersome computational workload unknowingly consumes a lot of dynamic response time, greatly impacting dynamic response performance.

Based on this, the research framework of this paper is shown in Figure 1. In this paper, a nonlinear ADRC method is proposed to improved robustness and stable control of the OER within the optimal range for enhanced control effectiveness. Conventional linear control methods face challenges in dealing with the nonlinear characteristics of fuel cells, necessitating the adoption of a more suitable approach. The ADRC method, which incorporates error feedback and effectively estimates disturbances in the system, is utilized as a more direct and effective control system for the air supply subsystem. The performance and robustness of the control strategy is verified by comparing the ADRC strategy with the PI control strategy. Models of the PEMFC and its controller are developed and simulated to validate the effectiveness of the proposed control method. The main contributions of this paper are summarized below:

- (1) A dynamic response model of the seventh-order PEMFC air supply subsystem is constructed to evaluate the effectiveness of the control strategy.
- (2) A nonlinear active anti-disturbance control method for the fuel cell gas supply system is proposed to evaluate the effectiveness of the control strategy and verified by simulation comparison.

The organizational structure of the article is as follows: Section 2 establishes the PEMFC gas supply system model to address the control issue of the OER. Section 3 analyzes the PI and ADRC strategies. Section 4 verifies the performance of the ADRC controller through simulation and discusses the simulation results. Finally, Section 5 presents the main conclusions.

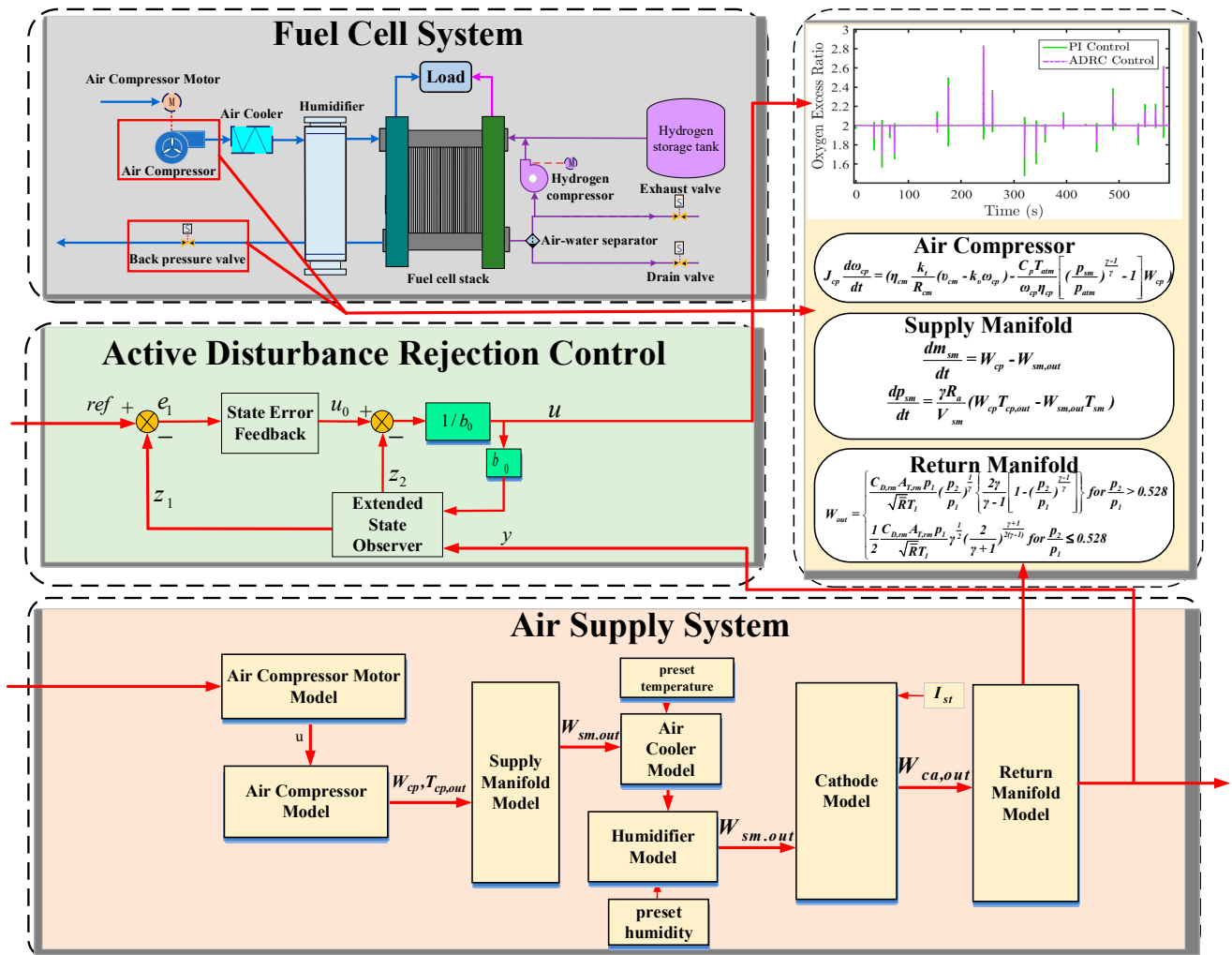


Figure 1. ADRC strategy framework based on extended state observer.

2. Modelling of PEMFC Air Supply Subsystem

The fuel cell air supply system model includes an air compressor, supply manifold, air cooler, humidifier, return manifold, and backpressure valve. The model assumes that the gases in the system follow the ideal gas law and that the temperature of the PEMFC stack can be adjusted to an optimal value. In addition, it is assumed that the temperature of the gas entering the stack is equal to the operating temperature of the stack. The intercooler is responsible for controlling the temperature at 353 K (Kelvin) and maintaining the humidity at 50%.

These assumptions form the basis for modeling and simulation of the PEMFC air supply system, allowing for its performance to be analyzed and optimized to deliver the required air to the stack while maintaining appropriate temperature and humidity levels.

2.1. Air Compressor Model

The model's input parameters include intake pressure $p_{cp,in}$, intake temperature $T_{cp,in}$, and motor voltage command v_{cm} ; downstream pressure is the pressure provided by the manifold $p_{cp,out} = p_{sm}$. In the typical configuration, the intake pressure and temperature are set to standard atmospheric pressure and ambient temperature, and engine control is one of the control signals of the fuel cell system and affects the operation of the air compressor. Downstream pressure is determined using multiple models that consider factors such as system requirements and load conditions.

When the air compressor receives an electrical signal through the motor command, the motor torque is adjusted accordingly. This change in torque directly impacts the performance of the compressor, affecting its output characteristics. The dynamic response of the air compressor model is a crucial aspect, enabling the system to adapt and regulate the air supply based on the specific demands of the fuel cell. This dynamic adjustment ensures that the fuel cell receives an appropriate and consistent air supply, optimizing its overall performance.

$$J_{cp} \frac{d\omega_{cp}}{dt} = (\eta_{cm} \frac{k_t}{R_{cm}} (v_{cm} - k_v \omega_{cp}) - \frac{C_p T_{atm}}{\omega_{cp} \eta_{cp}} \left[\left(\frac{p_{sm}}{p_{atm}} \right)^{\frac{\gamma-1}{\gamma}} - 1 \right] W_{cp}) \quad (1)$$

where k_t , R_{cm} , k_v represent the motor constant, while η_{cm} denotes the mechanical efficiency of the motor. These parameters are used to calculate the torque required to drive the compressor τ_{cp} . The specific heat capacity of air C_p is set to 1004, and the ratio of specific heat capacities γ is 1.4. J_{cp} is the moment of inertia of the compressor and motor combination, ω_{cp} represents the rotational speed of the compressor in radians per second (rad/s), and τ_{cm} is the torque input to the compressor motor.

2.2. Air Supply Manifold Model

The volumetric capacity of the supply manifold, which includes the volume occupied by the piping connecting the air compressor to the fuel cell stack, as well as the space occupied by the intercooler and humidifier, determines its capacity. Within the supply manifold, the air compressor supplies the incoming mass flow of air, while the outgoing mass flow relies on the flow at the manifold's exit.

$$\frac{dp_{sm}}{dt} = \frac{\gamma R_a}{V_{sm}} (W_{cp} T_{cp,out} - W_{sm,out} T_{sm}) \quad (2)$$

where V_{sm} represents the volume of the supply manifold, while T_{sm} represents the air temperature inside the supply manifold, which can be calculated using the ideal gas law with the help of m_{sm} and p_{sm} :

$$T_{sm} = \frac{P_{sm} V M_a}{m R} \quad (3)$$

2.3. Air Cooler Model

As a result of the elevated air temperature at the compressor's discharge, the temperature within the supply manifold rises correspondingly. To protect the fuel cell membrane from potential harm brought about by excessive heat, it becomes essential to lower the air's temperature prior to reaching the required operating temperature for the fuel cell stack. In this research, the impact of heat transfer was not considered. Hence, the intercooler is assumed to function optimally, maintaining the air temperature entering the stack at the designated level. It is also presumed that there is no pressure loss within the intercooler. Furthermore, given that temperature fluctuations can affect gas humidity, the humidity of the gas is determined after it exits the intercooler.

$$\phi_{cl} = \frac{p_{cl} \phi_{atm} p_{sat}(T_{atm})}{p_{atm} p_{sat}(T_{cl})} \quad (4)$$

where $p_{sat}(T_i)$ is the vapor saturation pressure, P_{cl} is the gas pressure in the intercooler, T_{cl} is the gas temperature through the intercooler, and $T_{cl} = T_{st}$.

The flow rate through the intercooler does not change: $W_{cl} = W_{sm,out}$.

2.4. Humidifier Model

During this procedure, the air processed by the intercooler is guided to the humidifier to elevate its humidity levels. Given that the humidifier is comparatively small, it can be included as a part of the supply duct's volume. For determining the alteration in air

humidity due to the added moisture during the humidification process, a static model of the humidifier is utilized. This should help mitigate any duplication concerns. This model assumes that the airflow temperature stays consistent. This assumption suggests that the water injected is either vapor or that any heat produced during water evaporation is already included in the intercooler. By taking these elements into account, the static model effectively estimates the variations in air humidity within the humidification system. These assumptions are based on the airflow conditions leaving the intercooler ($W_{cl} = W_{sm,out}$, p_{cl} , T_{cl} , ϕ_{cl}). The dry air mass flow rate at the humidifier inlet and outlet is kept constant:

$$W_{air,hm,in} = W_{air,hm,out} = W_{air,cl} \quad (5)$$

The flow rate out of the humidifier is regulated by the principle of conservation of mass:

$$W_{out} = W_{air,cl} + W_{v,hm} = W_{air,cl} + W_{v,cl} + W_{v,inj} \quad (6)$$

The output stream then enters the cathode of the fuel cell, and this outflow is the cathode inlet flow (ca, in).

2.5. Return Manifold Model

The temperature of the air discharged from the fuel cell stack typically tends to be lower compared to the air at the outlet of the air compressor. The flow rate into the return manifold $W_{ca,out}$ is as follows:

$$W_{ca,out} = k_{ca,out}(p_{ca} - p_{rm}) \quad (7)$$

where p_{ca} is the total cathode pressure, p_{rm} is the return manifold pressure (one of the model inputs), and k_{ca} is the orifice constant.

The equation for the gas pressure p_{rm} through the return manifold is as follows:

$$\frac{dp_{rm}}{dt} = \frac{R_a T_{rm}}{V_{rm}} (W_{ca} - W_{rm}) \quad (8)$$

The backpressure valve nozzle equation dictates the outlet mass flow rate of the return manifold.

$$\begin{cases} W = \frac{C_{D,rm} A_{T,rm} p_1}{\sqrt{R T_1}} \left(\frac{p_2}{p_1}\right)^{\frac{1}{\gamma}} \left\{ \frac{2\gamma}{\gamma-1} \left[1 - \left(\frac{p_2}{p_1}\right)^{\frac{\gamma-1}{\gamma}} \right] \right\} \text{ for } \frac{p_2}{p_1} > 0.528 \\ W_{choked} = \frac{1}{2} \frac{C_{D,rm} A_{T,rm} p_1}{\sqrt{R T_1}} \gamma^{\frac{1}{2}} \left(\frac{2}{\gamma+1}\right)^{\frac{\gamma+1}{2(\gamma-1)}} \text{ for } \frac{p_2}{p_1} \leq 0.528 \end{cases} \quad (9)$$

The area for opening the throttle can be fixed at a certain value or utilized as an extra variable for control to regulate the pressure in the intake manifold, subsequently impacting the pressure at the cathode. The key factors outlined in Table 1 are the main parameters for simulating the subsystem responsible for supplying air to the fuel cell.

Table 1. Main parameters of the PEMFC model.

Parameter	Unit	Value
T_{st}	K	353
d_c	m	0.2286
M_{O_2}	Kg/mol	0.032
k_{ca}	Kg/(s·Pa)	2.17×10^{-6}
F		
R_a	J/(kg·K)	298.6
V_{sm}	m ³	0.02
γ		1.4

Table 1. Cont.

Parameter	Unit	Value
C_p	J/(kg·K)	1004.88
J_{cp}	Kg·m ²	5×10^{-5}
k_v	V/(rad/s)	0.0153
k_t	N·m/A	0.0225
p_{atm}	bar	1
n_p		2
T_{atm}	K	298.15
R_{cm}	ohm	1.2
η_{cm}		0.98
$C_{D,rm}$		0.0124
\bar{R}	J/(mol K)	8.314
V_{sm}	m ³	0.02
η_{cp}		0.8

3. Controller Settings

To address the control issue of the OER, two simulation control tactics, PI and ADRC, are implemented.

3.1. PI Controller

The PI algorithm, which is a classical control method employed in the control strategy of PEMFC air supply systems, has gained widespread adoption owing to its simple structure, stability, and ease of implementation. The main advantages of PI controllers stem from the two actions they encompass, proportional (P) and integral (I), which collaborate within the control system to attain the desired system performance. In this paper, the PI control takes the step condition of the current as the perturbation input and the air compressor motor voltage as the control variable by using the PI control method; thus, the system can effectively track and maintain the oxygen excess rate and optimize the overall operation of the air supply system. Based on this, the constructed PI control model is shown in Figure 2.

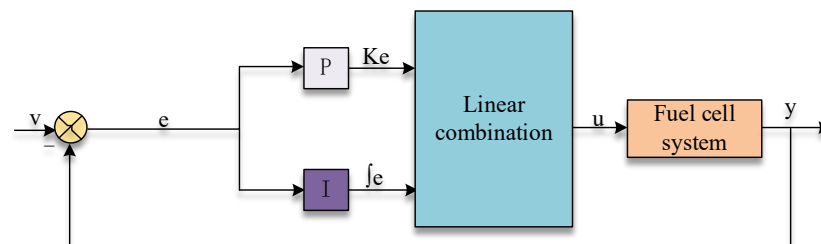


Figure 2. PI controller model.

For the PEMFC:

$$P + I \frac{1}{s} \quad (10)$$

3.2. ADRC Controller

In the realm of controlling methods for PEMFC air supply subsystems, the ADRC strategy presents a compelling alternative approach. At its core, the ADRC strategy relies on the utilization of an extended state observer capable of estimating both the internal state of the system and external disturbances. This comprehensive monitoring and feedback regulation enable effective control of the system.

One of the primary principles of the ADRC strategy is to enhance the system's robustness against uncertainties and external disruptions. By incorporating disturbance compensation, the ADRC algorithm enables the system to adapt to a wide range of unforeseen variations while maintaining stability and performance. The system's capability to

efficiently reject disruptions allows for it to maintain its intended performance levels even in the face of uncertainties and external disturbances. This ability ensures that, regardless of unforeseen challenges or outside interference, the system can continue to operate effectively and reliably. By consistently managing and mitigating the impact of these disruptions, the system can uphold its designed performance standards, thereby providing a robust solution in dynamic environments.

For the PEMFC:

$$\begin{cases} \dot{x} = Ax + Bu \\ y = Cx \end{cases} \quad (11)$$

Its classical observer system is $\dot{z} = Az - L(Cz - y) + Bu$. The two system error equations can be expressed as follows:

$$\begin{cases} \varepsilon = z - x \\ \dot{\varepsilon} = (A - LC)\varepsilon \end{cases} \quad (12)$$

When $A-LC$ is stable, $z(t)$ asymptotically approaches and estimates the state variable $x(t)$.

$$\begin{cases} \dot{x}_1 = x_2 \\ \dot{x}_2 = f(x_1, x_2, w(t), t) + bu \\ y = x_1 \end{cases} \quad (13)$$

where y is the output and is the observation; u is the control; and $f(x_1, x_2, w(t), t)$ is a multivariate function of state variables, external disturbances, and time. If $f(x_1, x_2, w(t), t)$ is known, such that $\varepsilon_1 = z - y$, then the state observer can be designed as follows:

$$\begin{cases} \dot{z}_1 = z_2 - \beta_{01}\varepsilon_1 \\ \dot{z}_2 = f(x_1, x_2, w(t), t) - \beta_{01}\varepsilon_1 + bu \end{cases} \quad (14)$$

In this equation, u is used as an input quantity to make the output of y match the desired value. When $f(x_1, x_2, w(t), t)$ is unknown, $f(x_1, x_2, w(t), t)$ is used as the full perturbation. To achieve a comprehensive observation of perturbations within the system, it is frequently required to introduce an extra variable into the observer. This design allows for the observer to not only monitor the system's state but also estimate the complete range of perturbations that impact the system's performance. By doing so, the observer becomes capable of more accurately reflecting the actual state of the system, even when confronted with intricate perturbations.

Then, Equation (13) can be rewritten as below:

$$\begin{cases} \dot{x}_1 = x_2 \\ \dot{x}_2 = x_3 + bu \\ x_3 = F(x_1, x_2, w(t), t) \\ y = x_1 \end{cases} \quad (15)$$

The dilated state observer can be constructed from u and y as follows:

$$\begin{cases} \dot{z}_1 = z_2 - \beta_{01}\varepsilon_1 \\ \dot{z}_2 = z_3 - \beta_{02}n_2(e) + b_0u \\ \dot{z}_3 = -\beta_{03}n_3(e) \end{cases} \quad (16)$$

where $z_i (i = 1, 2, 3)$ is the output, is the value of x_1, x_2 and the observed estimate of the full perturbation f ; $\beta_i (i = 1, 2, 3)$ is the value of the observer gain, which is an adjustable parameter.

From the control algorithm of ADRC, the basic expression form of ADRC design is as follows:

$$\dot{y} = f(x(t), \dots, w, t) + bu \quad (17)$$

Since b is uncertain, the above equation can be rewritten:

$$\dot{y} = F + b_0 u \tag{18}$$

where $n = f + (b - b_0)u$, and b_0 is the estimated value of b . Let $x_1 = y, x_2 = \dot{y}$; then, the above equation can be written as a state space expression:

$$\begin{cases} \begin{bmatrix} \dot{x}_1 \\ \dot{x}_2 \end{bmatrix} = \begin{bmatrix} 0 & 1 \\ 0 & 0 \end{bmatrix} \begin{bmatrix} x_1 \\ x_2 \end{bmatrix} + \begin{bmatrix} b_0 \\ 0 \end{bmatrix} u + \begin{bmatrix} 0 \\ 1 \end{bmatrix} \dot{n} \\ y = [1 \ 0] \begin{bmatrix} x_1 \\ x_2 \end{bmatrix} \end{cases} \tag{19}$$

Then, the corresponding dilated state observer is designed as below:

$$\begin{bmatrix} \dot{z}_1 \\ \dot{z}_2 \end{bmatrix} = \begin{bmatrix} -\beta_1 & 1 \\ -\beta_2 & 0 \end{bmatrix} \begin{bmatrix} z_1 \\ z_2 \end{bmatrix} + \begin{bmatrix} b_0 & \beta_1 \\ 0 & \beta_2 \end{bmatrix} \begin{bmatrix} u \\ y \end{bmatrix} \tag{20}$$

$$u = \frac{u_0 - z_2}{b_0} \tag{21}$$

Based on Equation (18) and $z_2 \sim F$, the system can be expressed as follows:

$$\dot{y} = F + b_0 u \approx F + b_0 \left(\frac{u_0 - F}{b_0} \right) = u_0 \tag{22}$$

The final model for the ADRC controller is shown in Figure 3:

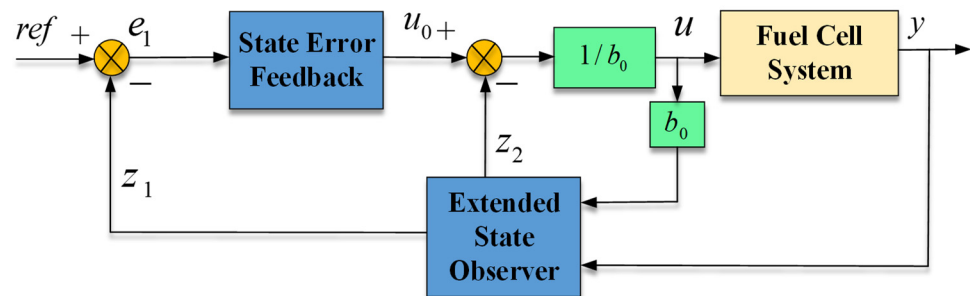


Figure 3. ADRC controller design.

4. Simulation and Results

In this paper, the test condition for the study involved selecting the load data obtained during the operation of the fuel cell system. To prevent oxygen deficiency under varying current conditions in the electric stack, the OER setting was fixed at a constant value of 2. This parameter setting enables the dynamic performance verification of the system. Figure 4 of this paper illustrates the current variation process of the fuel cell electro stack, with the simulation encompassing a current range of 100 A to 230 A.

Figure 5 displays the variation curve of the electro stack voltage, revealing that the ADRC produces smaller amplitude compared to PI control. The performance of OER regulation is illustrated in Figure 6, demonstrating that all control methods exhibit favorable dynamic tracking behavior when adjusting the OER to the set value. Specifically, the proposed ADRC controller achieves faster reaching of the set point without any overshoot, outperforming the PI controller, particularly when there is a change in the fuel cell current. Moreover, the ADRC method yields a dynamic response with reduced steady-state error. These results highlight the advantages of the ADRC controller in terms of speed and accuracy in regulating the OER under varying stacking current conditions.

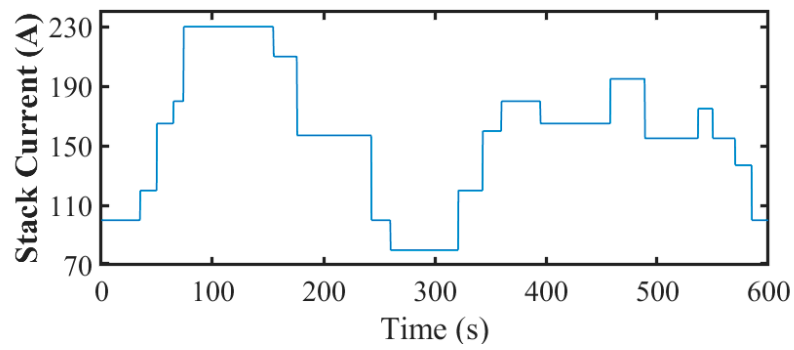


Figure 4. Setting of load current change in electric pile.

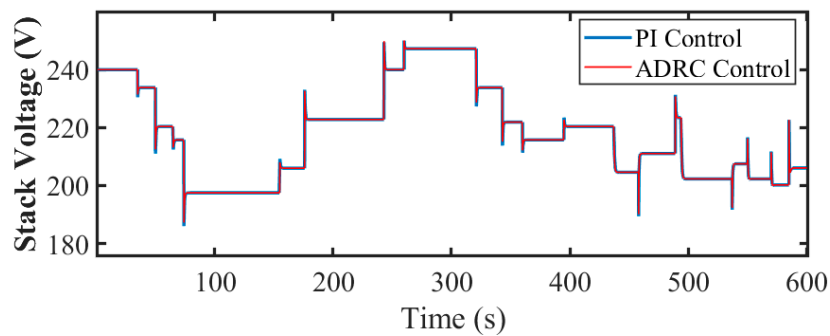


Figure 5. PI-controlled and ADRC-controlled fuel cell stack voltage curves.

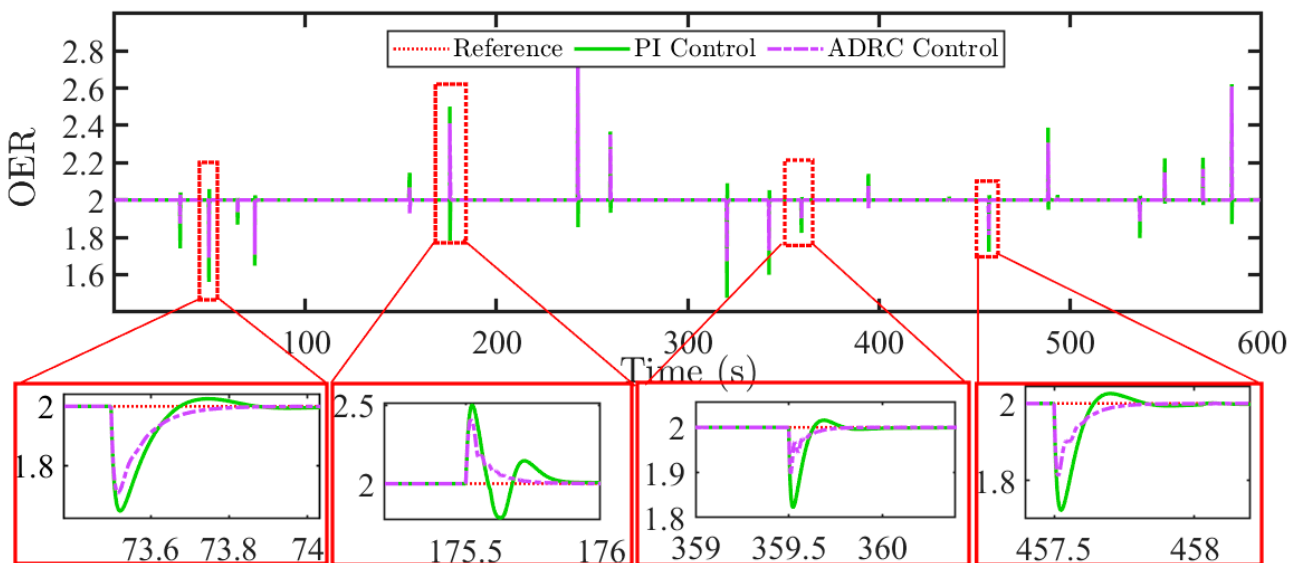


Figure 6. Response curve of peroxide ratio under PI control and ADRC.

Compared with PI, one of the most significant advantages of ADRC is its ability to reduce system state overshoot by generating virtual control signals that remove the transfer function’s zero point in relation to the system output. Figure 6 demonstrates that although the PI algorithm allows for the OER to achieve the reference value promptly, it also results in significant overshoot and oscillations. ADRC, on the other hand, has been shown to be effective in reducing overshoot. However, this advantage comes at the cost of some control capabilities, resulting in delayed system response. By utilizing an algorithmic framework, ADRC assesses the overall system disturbance across diverse frequency ranges, effectively mitigating system state overshoot while ensuring the OER tracks the reference swiftly and precisely. At the same time, the system control variable in the ADRC algorithm, particularly

the air compressor’s input voltage, shows minimal fluctuations, as illustrated in Figure 5. In contrast, the PI algorithm attempts to align the OER with the set reference value through a control variable with substantial variations, often resulting in system state overshoot. Conversely, ADRC keeps the system input signal variations within an acceptable boundary.

In the subsequent analyses, Figure 7a presents the transient tracking performance of the supply manifold pressure, whereas Figure 7b provides a zoomed-in plot within a 74–80 s time window. Figure 8a displays the transient tracking performance of the electric stack pressure P_{ca} , and Figure 8b offers a zoomed-in plot within a 430–444 s time window. As shown in Figure 8b, the ADRC controller, utilizing feedback control design, exhibits faster transient response performance and smaller error compared to PI controllers. When compared to the proposed controller, ADRC can achieve similar or superior control performance. ADRC effectively addresses interference between systems, actively manages disturbance problems, ensures high control accuracy, and offers a solution for feedback control in nonlinear systems.

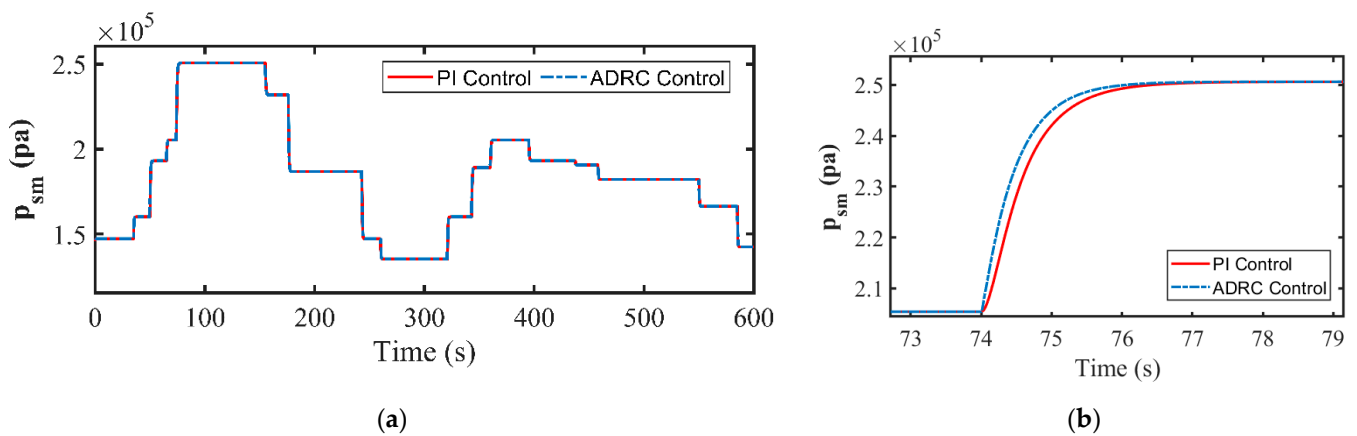


Figure 7. Simulation results of PI control and ADRC: (a) supply pipeline pressure tracking curve; (b) local zoomed-in view of supply pipeline pressure tracking curve under PI control and ADRC.

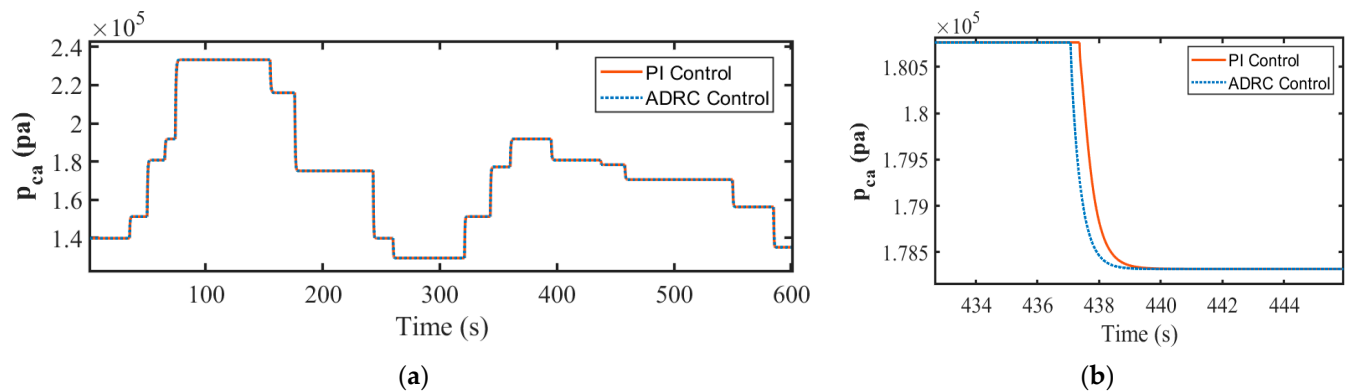


Figure 8. Simulation results of PI control and ADRC: (a) electric reactor pressure tracking curve; (b) local zoomed-in view of electric reactor pressure tracking curve.

As for Figure 9a, it illustrates the observed results of oxygen quality for both control methods, while Figure 9b provides a zoomed-in plot within a 396 s time window. At 395.05 s, the oxygen quality under PI control is 0.0019 kg, surpassing the system’s reference value. In contrast, the oxygen quality under ADRC is only 0.0018 kg, aligning closely with the system’s estimated value. Similarly, Figure 10a showcase the observed results of hydrogen quality for both control methods, with Figure 10b zooming in on a 396 s time window. Both observers can maintain the relative error in the range of 4% and 2% when observing the levels of oxygen and nitrogen content. It is evident that ADRC exhibits

smaller error, achieves steady state quicker than PI control, and does not exhibit a slight overshoot above the steady state value during transient states. ADRC demonstrates fast adjustment time and low estimation error, suggesting strong convergence.

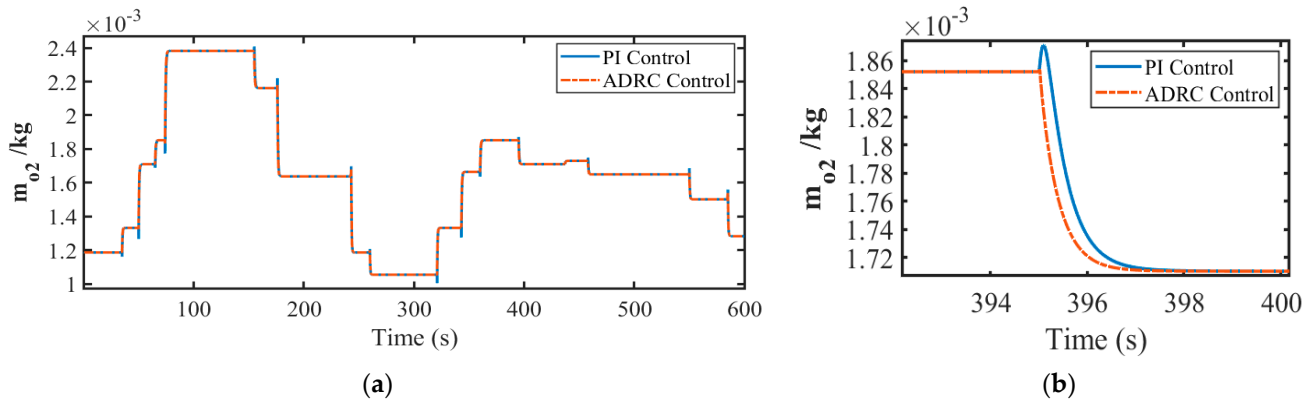


Figure 9. Simulation results of PI control and ADRC: (a) oxygen mass observation curve; (b) oxygen mass observation curve local zoomed in.

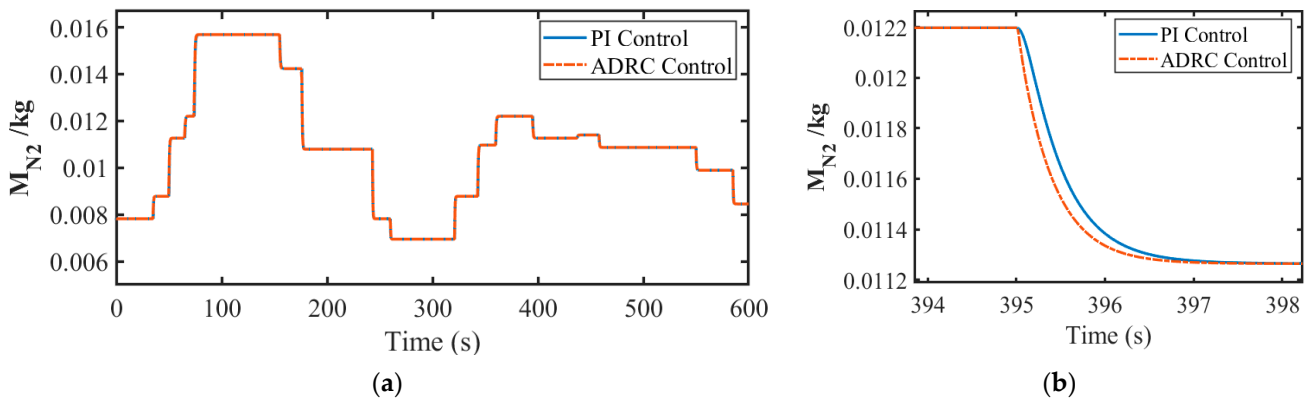


Figure 10. Simulation results of PI control and ADRC: (a) nitrogen mass observation curve; (b) nitrogen mass observation curve local zoomed in.

To evaluate the effectiveness of these control strategies, we identified three quantitative indicators for comparison: ISE, IAE, and TV. The calculations are shown in Equations (23)–(25), and the results are shown in Table 2, indicating that the control performance of the ADRC exceeds all evaluation criteria. Although the PI algorithm can make the OER quickly reach the reference value, it will also cause obvious overshoot and oscillation, which will lead to excessive ISE, IAE, and TV. By using the algorithm framework, ADRC evaluates different frequencies. The overall system disturbance within the range effectively alleviates the system state overshoot, while ensuring that the OER can quickly and accurately track the reference without generating excessive ISE, IAE, and TV. ADRC exhibits the smallest tracking error, an essential factor in control systems, as it indicates higher accuracy in following the desired output. Additionally, ADRC shows minimal control signal fluctuation, which is crucial for maintaining system stability and performance. On the other hand, the TV values for PI are significantly higher than those for ADRC, which could potentially lead to increased wear and tear on the air compressor, thereby shortening its lifespan.

Table 2. Evaluation and comparison of control performance.

Parameter	ADRC	PI
IAE	0.1942	0.502
ISE	0.058	0.1382
TV	351.4392	399.1248

The ADRC observes the system state and estimates the total perturbation by expanding the state observer on the one hand, which facilitates the real-time understanding of the system state; on the other hand, it can also compensate the perturbation in a timely manner in the form of feedback according to the overall amount of the role of the perturbation inside and outside the system model, which helps to improve the robustness of the system.

$$ISE = \int_0^{\infty} (v - y)^2 dt \quad (23)$$

$$IAE = \int_0^{\infty} |v - y| dt \quad (24)$$

$$TV = \sum_{i=1}^{\infty} |u_{i+1} - u_i| \quad (25)$$

where $|u_{i+1} - u_i|$ represents the step size of the voltage change within a control step.

One of the notable strengths of ADRC is the negligible overshoot resulting from observer error, a critical aspect in control systems where overshoot can lead to system instability and inefficiency. This analysis distinctly underscores ADRC's capability in reducing overshoot and enhancing response speed, attributes that are vital for efficient control system performance. Moreover, ADRC exhibits superior stability compared to PI, particularly in scenarios that involve simultaneous stepwise changes in load current set point. This makes ADRC a more reliable and robust choice for dynamic environments where load changes are frequent and unpredictable. Overall, the findings highlight ADRC's comprehensive benefits in improving the control system performance, stability, and lifespan of the air compressor.

The air supply subsystem of the fuel cell is inherently nonlinear, and in managing it, the ADRC exhibits quicker response times than PI control, with no overshooting. It can swiftly stabilize the system under different loads while also keeping a consistent OER value. While the PEMFC system operates smoothly, the voltage under ADRC mirrors the expected value, meeting the power needs of the vehicle. Thus, the proposed ADRC architecture is effective in improving the dynamic response performance and efficiency of the fuel cell system.

5. Conclusions

This paper introduces a nonlinear feedback control method for PEMFC air supply subsystems and draws the following conclusions:

Compared with the PI control strategy, the ISE value and IAE value of the ADRC strategy are reduced by 61.31% and 58.03%, respectively. From this point of view, the ADRC strategy shows a smaller tracking error in the steady-state operation process, and the control accuracy exceeds the PI control strategy. In addition, from the fact that the TV value of the ADRC strategy is smaller than that of the PI control strategy, the ADRC strategy can effectively reduce overshoot and faster transient response performance. ADRC is more suitable for the nonlinear characteristics of the gas supply system and can quickly respond to the OER reference setting value. Therefore, from the perspective of comprehensive performance, ADRC is obviously better than PI control and is more suitable for controlling PEMFC air supply systems.

Author Contributions: Conceptualization, J.Z. (Jiaming Zhou) and W.D.; methodology, J.Z. (Jiaming Zhou) and W.D.; software, J.Z. (Jinming Zhang) and G.W.; validation, J.Z. (Jiaming Zhou), J.Z. (Jinming Zhang) and F.Y.; formal analysis, C.Z.; investigation, G.W.; resources, J.Z. (Jiaming Zhou) and W.D.; data curation, Z.Z.; writing—original draft preparation, W.D.; writing—review and editing, J.Z. (Jiaming Zhou); visualization, F.Y. and J.Z. (Jinming Zhang); supervision, Z.Z.; project administration, F.Y.; funding acquisition, F.Y. All authors have read and agreed to the published version of the manuscript.

Funding: This research is supported by the Weifang University of Science and Technology High-level Talent Research Start-up Fund Project (KJRC2023001), the National Key Research and Development Program of China (2022YFE0137600), and the Weifang University of Science and Technology 2023 School-level Project (2023KJ02 and 2023KJ03).

Data Availability Statement: The data presented in this study are available on request from the corresponding author. The data are not publicly available due to third-party confidentiality agreement restrictions.

Conflicts of Interest: Author Guangping Wu was employed by the Zhongtong Bus Co., Ltd. The remaining authors declare that the research was conducted in the absence of any commercial or financial relationships that could be construed as a potential conflict of interest.

References

1. Yi, F.; Su, Q.; Feng, C.; Wang, X.; Yang, L.; Zhou, J.; Fan, Z.; Jiang, S.; Zhang, Z.; Yu, T.; et al. Response Analysis and Stator Optimization of Ultrahigh-Speed PMSM for Fuel Cell Electric Air Compressor. *IEEE Trans. Transp. Electrification*. **2023**, *9*, 5098–5110. [[CrossRef](#)]
2. Jia, C.; He, H.; Zhou, J.; Li, K.; Li, J.; Wei, Z. A performance degradation prediction model for PEMFC based on bi-directional long short-term memory and multi-head self-attention mechanism. *Int. J. Hydrogen Energy* **2024**, *60*, 133–146. [[CrossRef](#)]
3. Jia, C.; Zhou, J.; He, H.; Li, J.; Wei, Z.; Li, K. Health-conscious deep reinforcement learning energy management for fuel cell buses integrating environmental and look-ahead road information. *Energy* **2024**, *290*, 130146. [[CrossRef](#)]
4. Celik, E.; Karagoz, I. Investigation of the effects of intermediate reservoirs and intermediate feedings applications on the performance of proton exchange membrane fuel cells. *Fuel* **2023**, *339*, 126975. [[CrossRef](#)]
5. Bahari, M.; Rostami, M.; Entezari, A.; Ghahremani, S.; Etmnan, M. Performance evaluation and multi-objective optimization of a novel UAV propulsion system based on PEM fuel cell. *Fuel* **2022**, *311*, 122554. [[CrossRef](#)]
6. Sultan, H.M.; Menesy, A.S.; Hassan, M.; Jurado, F.; Kamel, S. Standard and Quasi Oppositional bonobo optimizers for parameter extraction of PEM fuel cell stacks. *Fuel* **2023**, *340*, 127586. [[CrossRef](#)]
7. Li, Q.; Yin, L.; Yang, H.; Wang, T.; Qiu, Y.; Chen, W. Multiobjective optimization and data-driven constraint adaptive predictive control for efficient and stable operation of PEMFC system. *IEEE Trans. Ind. Electron.* **2020**, *68*, 12418–12429. [[CrossRef](#)]
8. Pilloni, A.; Pisano, A.; Usai, E. Observer-based air excess ratio control of a PEM fuel cell system via high-order sliding mode. *IEEE Trans. Ind. Electron.* **2015**, *62*, 5236–5246. [[CrossRef](#)]
9. Su, Q.; Zhou, J.; Yi, F.; Hu, D.; Lu, D.; Wu, G.; Zhang, C.; Deng, B.; Cao, D. An intelligent control method for PEMFC air supply subsystem to optimize dynamic response performance. *Fuel* **2024**, *361*, 130697. [[CrossRef](#)]
10. Yue, H.; He, H.; Han, M.; Gong, S. Active disturbance rejection control strategy for PEMFC oxygen excess ratio based on adaptive internal state estimation using unscented Kalman filter. *Fuel* **2024**, *356*, 129619. [[CrossRef](#)]
11. Rodatz, S.; Paganelli, G.; Guzzella, L. Optimizing air supply control of a PEM fuel cell system. In Proceedings of the 2003 American Control Conference, Denver, CO, USA, 4–6 June 2003; pp. 2043–2048.
12. She, Y.; Baran, M.E.; She, X. Multiobjective control of PEM fuel cell system with improved durability. *IEEE Trans. Sustain. Energy* **2012**, *4*, 127–135. [[CrossRef](#)]
13. Bianchi, F.D.; Kunusch, C.; Ocampo-Martinez, C.; Sánchez-Peña, R.S. A gain-scheduled LPV control for oxygen stoichiometry regulation in PEM fuel cell systems. *IEEE Trans. Control Syst. Technol.* **2013**, *22*, 1837–1844. [[CrossRef](#)]
14. Gruber, J.; Bordons, C.; Oliva, A. Nonlinear MPC for the airflow in a PEM fuel cell using a Volterra series model. *Control Eng. Pract.* **2012**, *20*, 205–217. [[CrossRef](#)]
15. Laghrouche, S.; Harmouche, M.; Ahmed, F.S.; Chitour, Y. Control of PEMFC air-feed system using Lyapunov-based robust and adaptive higher order sliding mode control. *IEEE Trans. Control Syst. Technol.* **2014**, *23*, 1594–1601. [[CrossRef](#)]
16. Laghrouche, S.; Liu, J.; Ahmed, F.S.; Harmouche, M.; Wack, M. Adaptive second-order sliding mode observer-based fault reconstruction for PEM fuel cell air-feed system. *IEEE Trans. Control Syst. Technol.* **2014**, *23*, 1098–1109. [[CrossRef](#)]
17. Ma, Y.; Zhang, F.; Gao, J.; Chen, H.; Shen, T. Oxygen excess ratio control of PEM fuel cells using observer-based nonlinear triple-step controller. *Int. J. Hydrogen Energy* **2020**, *45*, 29705–29717. [[CrossRef](#)]
18. Abbaker AM, O.; Wang, H.; Tian, Y. Adaptive integral type-terminal sliding mode control for PEMFC air supply system using time delay estimation algorithm. *Asian J. Control* **2022**, *24*, 217–226. [[CrossRef](#)]

19. Hu, Y.; Chen, H.; Gong, X.; Yu, S.; Gao, J.; Chen, H. Control-oriented modeling and robust nonlinear triple-step controller design for an air-feed system for polymer electrolyte membrane fuel cells. *Asian J. Control* **2019**, *21*, 1811–1823. [[CrossRef](#)]
20. Liu, J.; Laghrouche, S.; Ahmed, F.-S.; Wack, M. PEM fuel cell air-feed system observer design for automotive applications: An adaptive numerical differentiation approach. *Int. J. Hydrogen Energy* **2014**, *39*, 17210–17221. [[CrossRef](#)]
21. Liu, J.; Gao, Y.; Su, X.; Wack, M.; Wu, L. Disturbance-observer-based control for air management of PEM fuel cell systems via sliding mode technique. *IEEE Trans. Control Syst. Technol.* **2018**, *27*, 1129–1138. [[CrossRef](#)]
22. Wu, J.; Zhao, J.; Liu, Z.; Yang, H. Parameter estimation and control of a fuel cell air supply system based on an improved extended state observer. *Energy Sources Part A Recovery Util. Environ. Eff.* **2024**, *46*, 362–378. [[CrossRef](#)]
23. Deng, Z.; Chen, M.; Wang, H.; Chen, Q. Performance-oriented model learning and model predictive control for PEMFC air supply system. *Int. J. Hydrogen Energy* **2024**, *64*, 339–348. [[CrossRef](#)]
24. Wei, L.; Zhu, X.; Wang, X.; Hu, Z.; Wang, M. Research on the coordinated control of oxygen excess ratio and air pressure for PEMFC's air supply system. *Int. J. Hydrogen Energy* **2024**, *69*, 122–133. [[CrossRef](#)]
25. Jia, C.; He, H.; Zhou, J.; Li, J.; Wei, Z.; Li, K. Learning-based model predictive energy management for fuel cell hybrid electric bus with health-aware control. *Appl. Energy* **2024**, *355*, 122228. [[CrossRef](#)]
26. Qi, Y.; Espinoza-Andaluz, M.; Thern, M.; Li, T.; Andersson, M. Dynamic modelling and controlling strategy of polymer electrolyte fuel cells. *Int. J. Hydrogen Energy* **2020**, *45*, 29718–29729. [[CrossRef](#)]
27. Deng, Z.; Chen, Q.; Zhang, L.; Fu, Z.; Zhou, K. Weighted fusion control for proton exchange membrane fuel cell system. *Int. J. Hydrogen Energy* **2020**, *45*, 15327–15335. [[CrossRef](#)]
28. Jia, C.; Li, K.; He, H.; Zhou, J.; Li, J.; Wei, Z. Health-aware energy management strategy for fuel cell hybrid bus considering air-conditioning control based on TD3 algorithm. *Energy* **2023**, *283*, 128462. [[CrossRef](#)]

Disclaimer/Publisher's Note: The statements, opinions and data contained in all publications are solely those of the individual author(s) and contributor(s) and not of MDPI and/or the editor(s). MDPI and/or the editor(s) disclaim responsibility for any injury to people or property resulting from any ideas, methods, instructions or products referred to in the content.